

# WAYS OF IMPROVING OF ACTIVE CONTOUR METHODS IN COLONOSCOPY IMAGE SEGMENTATION

RANEEM ISMAIL ✉, SZILVIA NAGY

Széchenyi István University, Egyetem tér 1, Győr 9026, Hungary.  
e-mail: raneem.ismail@hallgato.sze.hu, nagysz@sze.hu

(Received July 16, 2021; revised November 18, 2021; accepted January 11, 2022)

## ABSTRACT

As colonoscopy is the standard screening approach for colorectal polyps, and the first step of the correct classification and the efficient automatic diagnostics is the accurate detection and segmentation of the existing polyps, it is worth researching systematically, how colonoscopy databases are responding to two of the most influential variational segmentation methods, the geodesic and Chan–Vese active contour methods. Due to the quality variation of the colonoscopy databases, pre-processing steps are made. Then, 14 various filtered images are evaluated as different inputs for the active contour methods using the Sørensen–Dice Similarity Coefficient as a performance measurement metric. The effects of the initial mask shape and its size together with the number of iterations, contraction bias and smoothness factor are studied. In general, the Chan–Vese method showed more efficiency to match the actual contour of the polyp than the geodesic one with an initial mask possibly located within the polyp area. Preprocessing such as reflection removal, background subtraction and mean or median filtering can improve the Sørensen–Dice coefficient by up to 0.5.

Keywords: active contour segmentation methods, Chan–Vese method, colonoscopy image, geodesic method, Sørensen–Dice Similarity Coefficient.

## INTRODUCTION

Image segmentation is one of the most studied branches in image processing field which is used to segregate the meaningful regions of interest that have common characteristics from the other components of the image, to make the subsequent processing steps more efficient (Ismail and Nagy, 2021).

Segmentation methods are generally classified into two main categories which are edge-based and region-based segmentation methods. Edge-based methods use the discontinuities in the local properties like (brightness, color, or texture) as a criterion for determining the boundaries of the regions to be segmented, such as Canny approach (Canny, 1986) that depends on the detection of discontinuities in the brightness to build the connected curves. Region-based methods based on grouping pixels of similar local properties to define the boundaries of the areas to be segmented, like region growing (Adams and Bischof, 1994) and region merging (Brice and Fennema, 1970) approaches. The lack of a clear optimization criterion in such algorithms limits their successful use in more difficult tasks. Nevertheless, these methods paved the way for using more effective approaches based on energy constraints and forces in the

image for separation the region of interest using some variational principle (Ismail and Nagy, 2021).

Variational methods aim to find a closed contour that divides the image into subregions. To this end, a minimizing of an energy functional is required, which results in a partial differential equation. The solution of this equation identifies a meaningful representation of the image. By the end of the 80's, the first variational formulations for image segmentation appeared, especially, the Snakes approach by Kass, Witkin, and Terzopoulos in 1988 (Kass *et al.*, 1988) which is an edge-based segmentation method, and the Mumford-Shah formulation in 1989 (Mumford and Shah, 1989) which is a region-based segmentation method.

Recently, medical image segmentation based on active contour methods has acquired more concern from researchers. Yang and Jiang (2020) constructed a new level set model based on non-local means (NLM) filtering with a new edge-stop criterion. A partially automatic hybrid active contour method using a local bias correction function and probability score was proposed in (Fang *et al.*, 2020) for segmentation of 2D ultrasound images with noise, blurry boundaries, and intensity heterogeneity. In the field of retinal fundus images, Bhat and Kumar (2019) introduced a three phases approach

to segment the optic disc, a localized active contour step was used for the 3rd, refined segmentation. Colonoscopy images also gain the close cooperation of several disciplines researchers and will be the field of practical application for this article.

Colorectal cancer (CRC) is the third lethal cancer type and the fourth most common cause of cancer mortality worldwide, (depending on the year and the country where the statistics took place) (Ismail and Nagy, 2021; Nguyen *et al.*, 2020). To reduce the risk of the benign polyps evolving into any kind of cancerous lesions, gastroenterologists recommend regular screening of the colorectal tract. By early detection, they will be able to classify and remove the abnormal lesions in a safe time, and colonoscopy is the most applicable method for these purposes.

The segmentation procedure is the first step of any polyp classification system; therefore, it directly affects the accuracy of the final classification results. There are basic challenges with the polyp segmentation topic, which must be processed; such as the narrow colour spectrum, the richness in textures, blood vessels, and heterogeneous regions, and the existence of specular highlights as a result of the colonoscope light source reflections. Furthermore, the diversity of polyps' categories according to their elliptical variable shapes, sizes, colors, viewing angle, and even the micro-architecture of epithelial pits the so-called pit patterns pose another interesting challenge. Moreover, the edges of the polyps are of varying strength because of the difference in the lesions' morphology and their growth location into or onto the bowel wall.

Recently, using active contour methods is efficiently present in the colonoscopy image segmentation field. In (Georgieva *et al.*, 2017; 2018; Sasmal *et al.*, 2018; Dutta *et al.*, 2018) researchers used an active contour without edges approach, i.e., Chan–Vese segmentation model to construct segmentation schemes for polyps with poor edges, i.e., not strong enough edges. The proposed methods were accompanied by various pre-processing steps and different evaluation metrics.

In the following considerations, we aim to systematically evaluate the performance of the geodesic and Chan–Vese methods with colonoscopy images as two of the most efficacious variational segmentation methods. Due to the complicated bowel environment and the non-uniform characteristics of the polyps, in addition to the variations of the polyps' edge strength, it is interesting to study and compare the applicability of these two methods especially because they have two different work mechanisms. Practically, random image samples of ETIS-Larib Polyp DB (Juan *et al.*, 2014), CVC-

ColonDB (Bernal *et al.*, 2012), and CVC-ClinicDB (Bernal *et al.*, 2015) databases are tested, and the results are evaluated using the Sørensen–Dice Similarity Coefficient measurement (Dutta *et al.*, 2018; Taha and Hanbury, 2015; Carass *et al.*, 2020). Each of the calculations starts from a rough initial mask – rectangular or circular–, based on the ground truth mask of the image database that can be the output of any of the existing polyp localization methods (Juan *et al.*, 2014; Nagy *et al.*, 2017; Yuji *et al.*, 2015; Bernal *et al.*, 2017).

The article is organized as follows. In the next section, the mathematical background of the active contour methods is shortly summarized. Also, the circumstances in our experiments, the evaluation criteria are given in the same section, in Materials and Methods. Next, in Section Results, the results of the calculations are given with short analysis. The concluding discussion is presented in the last section, and some of the detailed results are given in tables in an appendix.

## MATERIALS AND METHODS

### ACTIVE CONTOUR METHODS – MATHEMATICAL BACKGROUND

Active contour was one of the first variational approaches for image segmentation and it is considered among the most effective models. It was first introduced by Kass, Witkin, and Terzopoulos in 1988 (Kass *et al.*, 1988), and since then, it has been developed and modified by many researchers (Caselles *et al.*, 1997; Chan and Vese, 2000; 2001). The classical snake approach is briefly summarized as follows. First, the active contour is defined by drawing an initial mask near to the object to be segmented. Then, the contour will move towards a more optimal place by decreasing its energy in each sequential step, and at the same time, it will try to comply with both the energy constraints which affect its shape characteristics (like length, stiffness, elasticity) and the constraints related to the properties of the image. Finally, the snake will iteratively evolve to reach the minimum of the cost function and match the object of interest (Ismail and Nagy, 2021).

In (Kass *et al.*, 1988), the authors proposed to minimize an energy functional consists of internal and external energies and has the following mathematical formulation

$$E(C) = E_{\text{int}}(C) + E_{\text{ext}}(C) = \int_0^1 \left\{ \frac{\alpha}{2} |C_s(s)|^2 + \frac{\beta}{2} |C_{ss}(s)|^2 \right\} ds - \int_0^1 |\nabla I(C(s))|^2 ds, \quad (1)$$

where,  $I: \Omega \subset \mathbb{R}^2 \rightarrow \mathbb{R}$  is the input image, and  $C: [0,1] \rightarrow \Omega$  denotes a parametric curve on a grid  $\Omega$ . The

weights  $\alpha \geq 0$  and  $\beta \geq 0$  deal with the elasticity and the stiffness of the curve respectively.  $C_s$  and  $C_{ss}$  mean the first and second derivative of the curve  $C$  with respect to its parameter  $s$ . Minimizing the total energy function will create short, smooth, and stiff curves while passing through locations with the largest gradient values  $|\nabla I|$ .

In 1989, the mathematicians Mumford and Shah (Mumford and Shah, 1989) proposed to compute the segmentation of the input image by minimizing the following cost functional

$$E(u, C) = \int_{\Omega} (I(x) - u(x))^2 dx + \lambda \int_{\Omega/C} |\nabla u(x)|^2 dx + \nu |C|. \quad (2)$$

It concerns the piecewise smooth approximation  $u: \Omega \rightarrow R$  of the input image  $I$ , in addition to a one-dimensional discontinuity set  $C \subset \Omega$ . The first term confirms that  $u$  is a convenient approximation of the input image  $I$ , the second term, with weight  $\lambda > 0$ , confirms that the entire  $u$  is smooth except for the boundary discontinuity set  $C$ , and the last term, with weight  $\nu > 0$ , limits the minimal length of discontinuity set.

At the beginning of the 90's, many research papers related to image segmentation using Level Set Methods (LSMs) were published. LSMs are significant tools for numerical analysis and representation of curves, shapes, and surfaces. Their concept was first published in 1979 by Dervieux and Thomasset (Dervieux and Thomasset, 1979), and subsequently reinvented in 1988 by Osher and Sethian (Osher and Sethian, 1988). Their application has become common in the image segmentation and curves evolution related domains. The topological changes of the curve are treated automatically since the temporal evolution of a curve  $C(t)$  is implicitly represented using the zero level set of a Lipschitz function  $\phi(x, t)$  with a parameterization free formulation, such that

$$C(t) = \{x \in \Omega \mid \phi(x, t) = 0\}. \quad (3)$$

Using LSMs two different approaches based on the previously discussed variational models were presented. The first approach was introduced in 1997 by (Caselles, Kimmel, and Sapiro) known as the geodesic active contours (Caselles *et al.*, 1997; Kichenassamy *et al.*, 1995). The geodesic model was proposed to find a level set representation for the snake model, therefore, it is an edge-based segmentation method. It works on deriving the gradient descent equation for the curve and executing it using the level set equation. It is mathematically formulated as follows

$$\frac{\partial C(t)}{\partial t} = g(I)\kappa \bar{N} - (\nabla g \cdot \bar{N})\bar{N}, \quad (4)$$

where  $g(I)$  is the stopping criterion that limits the contour evolution and stops it when the contour gets close enough to the desired edge,  $\kappa = \text{div} \frac{\nabla \phi}{|\nabla \phi|}$  is the Euclidean curvature, and  $\bar{N}$  is the unit inward normal. Representing the previous equation using the level set equation will be as follows

$$\begin{aligned} \frac{\partial \phi}{\partial t} = |\nabla \phi| \text{div} \left( g(I) \frac{\nabla \phi}{|\nabla \phi|} \right) = \\ g(I) |\nabla \phi| \text{div} \left( \frac{\nabla \phi}{|\nabla \phi|} \right) + \nabla g(I) \cdot \nabla \phi, \end{aligned} \quad (5)$$

where  $\phi$  is a Lipschitz function representing the curve  $C$  as a zero level set.

The second approach was as an alternative to the edge-based methods, Chan and Vese proposed a two-phase region-based segmentation method known as active contour without edges (Chan and Vese, 2000; 2001). This approach reformulates the variational principle of the piecewise constant Mumford-Shah model using the level set method. Compared to the original Mumford-Shah model, Chan and Vese defined a new term to penalize the enclosed area of the curve, and made  $u$  as a function taking only two values

$$u = \{c_1 \text{ inside}(C)\}, u = \{c_2 \text{ outside}(C)\}. \quad (6)$$

The Chan-Vese segmentation is obtained by finding the best local minimizer of the following energy functional

$$E(c_1, c_2, C) = \mu \cdot \text{Length}(C) + \nu \cdot \text{Area}(\text{inside}(C)) + \lambda_1 \int_{\text{inside}(C)} |I(x, y) - c_1|^2 dx dy + \lambda_2 \int_{\text{outside}(C)} |I(x, y) - c_2|^2 dx dy, \quad (7)$$

where  $C$  is the curve that splits the image  $I$  into two regions of nearly constant intensity, the constants  $c_1$  and  $c_2$  are the averages of  $I$  inside and outside the contour  $C$  respectively, and  $(\mu \geq 0; \nu \geq 0; \lambda_1, \lambda_2 > 0)$  are fixed parameters. The first term controls the regularity of the curve by penalizing its length, while the size of the enclosed area of the curve is controlled by the second term, and the third and fourth terms are used to penalize the discrepancy between the piecewise constant model  $u$  and the input image  $I$ . After that, the authors suggested solving the minimization problem by using LSMs to implicitly represent the contour as a zero-crossing of a level set function (Chan and Vese, 2000; 2001).

## SIMULATION ENVIRONMENT AND DATABASES

The formulated steps were implemented by computer simulation in a MATLAB environment. We performed image processing, analysis, and visualizing using the powerful image processing toolbox. The experiments were conducted on the three databases ETIS-Larib Polyp DB (Juan *et al.*, 2014), CVC-ColonDB (Bernal *et al.*, 2012), and CVC-ClinicDB (Bernal *et al.*, 2015). They consist of 380, 195, and 612 images of size  $574 \times 500$ ,  $1225 \times 966$ , and  $384 \times 288$  pixels respectively. In addition to the colonoscopy images, masks corresponding to the regions covered by the polyps in the images are also included in the databases.

## EVALUATION CRITERIA

To evaluate the results of the active contour segmentation methods, we selected the Sørensen–Dice Similarity Coefficient as a performance measurement metric. The Sørensen–Dice index (SDI) is a widely applied metric for quantitatively validating of medical image segmentation algorithms. Moreover, it directly compares between the resulted segmented area and the mask provided in the database, i.e., the so called ground-truth mask (Dutta *et al.*, 2018; Taha and Hanbury, 2015; Carass *et al.*, 2020). It is mathematically computed as

$$Dice(A, B) = \frac{2 \times |A \cap B|}{|A| + |B|}, \quad (8)$$

in our case,  $A$  represents the active contour output binary segmented area and  $B$  represents the ground-truth mask.

## RESULTS

### REFERENCE CASE

As a reference case in this paper, geodesic and Chan–Vese active contour methods were tested on the 2D grayscale version of the colonoscopy original image and its original mask. Since the initial mask plays a critical role in the contour evolution and the accuracy of the segmentation process, we generated our own initial mask based on the corresponding given mask in the related database. It was a rectangle that encompasses the polyp area, to simulate the output of a previous, rough polyp localization method. The active contour default settings were selected, which are the following. The number of iterations was 100, smoothness factor was 1

and 0, and the contraction bias was 0.3 and 0 for the geodesic and the Chan–Vese active contours respectively. Table 1 lists the Sørensen–Dice Coefficient for the image samples from the three databases.

Table 1. *Sørensen–Dice Coefficient for the image samples in the reference case*

Database	Image Number	Geodesic	Chan–Vese
ETIS-Larib Polyp DB	49	0.8688	0.6771
	65	0.8922	0.7111
	135	0.8659	0.3950
	185	0.8702	0.6350
CVC-Colon Polyp DB	28	0.9225	0.7442
	67	0.9097	0.6016
	150	0.8832	0.7116
	202	0.9235	0.4318
CVC-Clinic Polyp DB	127	0.8865	0.5657
	151	0.9330	0.6524
	302	0.8583	0.6073
	405	0.8968	0.6512

The reference case results showed that the geodesic method performs better than the Chan–Vese method using the first default settings. Moreover, the geodesic initial mask showed a tendency to shrink or contract towards the polyp, while the Chan–Vese initial mask tend to grow or expand outwards, away from the polyp. It is also worth mentioning that the geodesic segmented area has an irregular almost rectangular shape. Consequently, the contour fails to mimic the exact smooth and elliptical polyp shape. Fig. 1 represents the reference case segmentation results of the grayscale version from image (28) in CVC-ColonDB database (Bernal *et al.*, 2012). To enhance the segmentation accuracy, we suggested a series of main pre-processing steps and studied their effect in comparison with the reference case results.

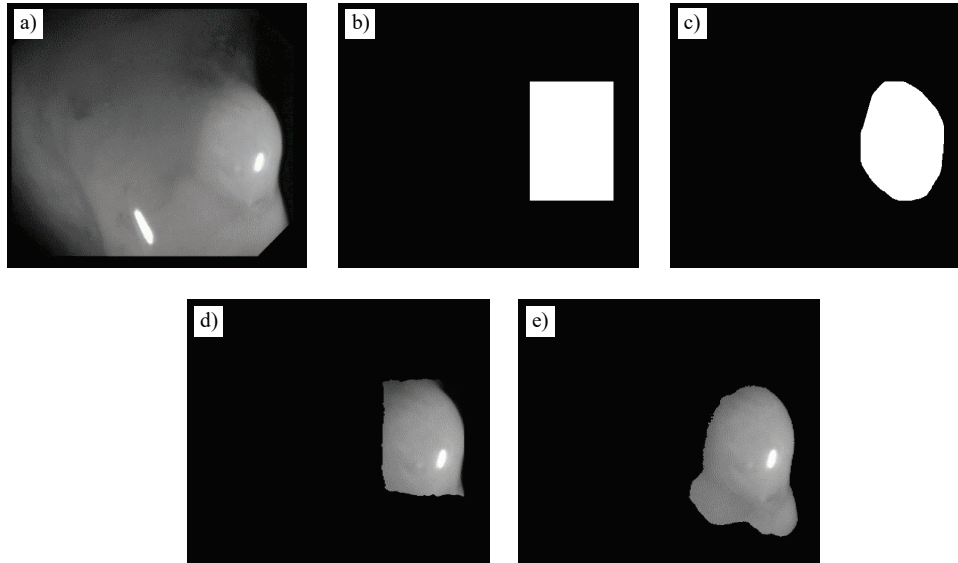


Fig. 1. The reference case segmentation results of the grayscale version from image (28) in CVC-ColonDB database (Bernal *et al.*, 2012). (a) The original image, (b) the given database mask, (c) the generated initial mask, (d) the geodesic segmented area, and (e) the Chan–Vese segmented area.

### PRE-PROCESSING PHASE

The following image pre-processing steps were carried out on all the colour channels to make the images more segmentable (Nagy *et al.*, 2020). First, the black frames of the images were cut off to reduce unnecessary information, then the reflections were smoothened into their environment together with a histogram stretching the following way. As all the images contained remainings of the frames at the corners, there was a large black peak at the black side of the image histogram; these pixels were collected into a black mask. As all the pictures contained bright whitish reflections, there was a peak, lower in magnitude, but much broader in width at the other, white side of the histogram, too. The pixels with this intensity were collected into a white mask. The middle part of the image histogram that was the useful information part, was stretched to the 0-255 intensity domain linearly.

We carried out the following 2 steps on the reflection pixels to smoothen them into their environment. First, the white or reflection mask was extended to its neighbouring pixels, if the average of the unmasked environment of the given pixel was much smaller than the actual pixel value. Second, the pixels in the reflection domains (inside the extended white mask) were substituted by the average of their unmasked environment (only those pixels counted into the environment, where neither the white, nor the black masks were present).

As a last step a large-scale average of the image, i.e., the background, was subtracted to provide a more even density distribution, where only the patterns that are of

the same size-scale of the expected polyps are visible, the larger tendencies are washed out. This step of course was together with a histogram stretching. Fig. 2 demonstrates these pre-processing steps for image (127) in CVC-ClinicDB database (Bernal *et al.*, 2015).

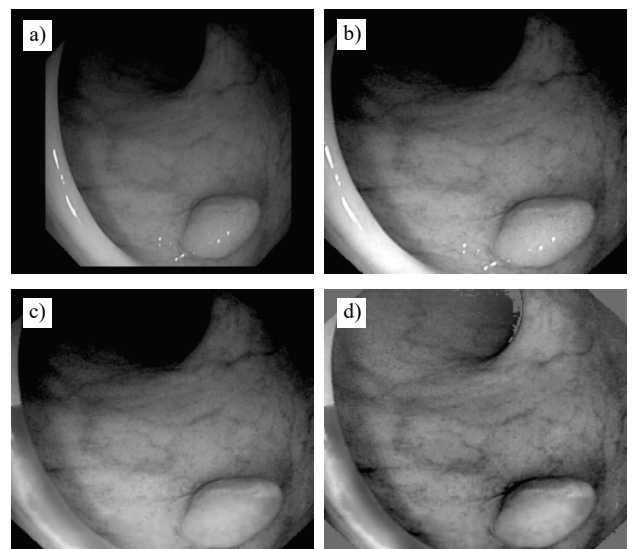


Fig. 2. The pre-processing steps of image (127) in CVC-ClinicDB database (Bernal *et al.*, 2015). (a) The original image, (b) the image with the frame cut-off and histograms stretched, (c) the removed reflection image, and (d) the background subtracted image.

### POST PRE-PROCESSING CASE

Since the characteristics of the databases are not uniform, and the applicability of the segmentation methods varies according to the used pictures, it is a field of

interest to test, whether pre-filtering influences the performance of the segmentation. In addition to the background subtracted image, different pre-filtering methods outputs were studied and tested as input images for the active contour methods.

There are several points that are taken into consideration when choosing some of the filtering techniques to be performed. The colonoscopy pictures are usually rather noisy, thus reduce noise components may yield more appropriate segmentation results. Certain linear filters, such as mean or Gaussian filters, are suitable for this purpose. In some cases, it is important to reduce the noise in an image and preserve the edges simultaneously, this could be useful for the geodesic method which is an edge-based segmentation method. The median filter has much less sensitivity to the outliers than the mean filter, consequently, the median filter removes these outliers without reducing the image edges strength. In addition to the median filter, the Wiener filter has the same ability to decrease the noise level and maintain edges at the same time. Moreover, some of the denoising filters make the images also blurrier with smoother edges which could be beneficial for the Chan–Vese method, since it looks for a smooth contour between objects of varying intensity to start the segmentation process.

The first group of filters was the simplest statistical filters, each of the mean, median, and standard deviation filters was included. In addition to these, the difference between the mean and the median was also tested, because it gives some detailed information about rapidly changing parts of the image (Ismail and Nagy, 2021).

As gradients are the basis of many edge detecting methods and their values are higher around large variations, i.e., around edges, thus the second suggested group of filters was the gradients. The gradient magnitude, the gradient direction, and the  $x$  and  $y$  direction components of the gradient were implemented.

The third group of filters was relatively distinctive; it is based on the Rényi entropies (Rényi, 1960) of the image, which are generalization of the famous Shannon entropy  $S_1$  (Shannon, 1948), and given by

$$S_n = \frac{1}{1-n} \ln \left( \sum_{i=1}^N I_i^n \right), \quad (9)$$

where  $I_i$  denotes the  $i^{\text{th}}$  pixel intensity normalized to be a probability distribution component. The structural entropy  $S_{str} = S_1 - S_2$ , and the spatial filling factor

$\ln q = S_0 - S_2$  are used to characterize the probability distributions shape (Shannon, 1948; Pipek *et al.*, 1992) so they were applied as well. The filter size was  $5 \times 5$  for the three filters groups previously listed.

The Gaussian filter with a standard deviation of 0.5, and the Wiener filter with a neighborhood size  $3 \times 3$  were also applied as the last two filtering options.

Practically, the 2D grayscale version of the background subtracted image and its fourteen filtered images were evaluated as different input pictures for the geodesic and Chan–Vese active contour methods. We kept using the rectangular initial mask with the same active contour default settings.

Compared to the reference case, the results confirmed that applying consecutive pre-processing steps and using background subtracted versions of the original colonoscopy images were highly beneficial and improved the segmentation results in most samples using the Chan–Vese method (in 9 samples out of 12 samples). Whereas the geodesic method results showed that (just 5 samples out of 12 samples) were positively affected by the preprocessing steps. It was observed that the Sørensen–Dice Coefficient values for the remaining image samples decreased just a little bit compared to the reference case. Moreover, in some samples, pre-processing produced images with smoother edges, and this somewhat negatively affected the performance of the edge-based geodesic method. The former results are clearly illustrated by comparing the Sørensen–Dice Coefficient values of using the background subtracted image and the rectangular mask in each of the three tables listed in the appendix with the corresponded reference case results.

On the other hand, the results of the pre-filtering methods proved the superior performance of the geodesic and Chan–Vese active contour methods with mean, median, Gaussian, and Wiener filters in almost all samples. Furthermore, the Chan–Vese segmented area matches the elliptical polyp borders very well. In contrast, the geodesic one still far from the ideal requested shape. In spite of the nearly identical performance of the geodesic method with almost all filters, for our next steps, we will keep on just the previously mentioned filters i.e., mean, median, Gaussian, and Wiener filters, because of the good segmentation results achieved with these filters for both geodesic and Chan–Vese methods. Fig. 3 and Fig. 4 give the resulting masked image for the background subtracted image (65) in ETIS-Larib Polyp DB database (Juan *et al.*, 2014) using the geodesic and Chan–Vese methods respectively.

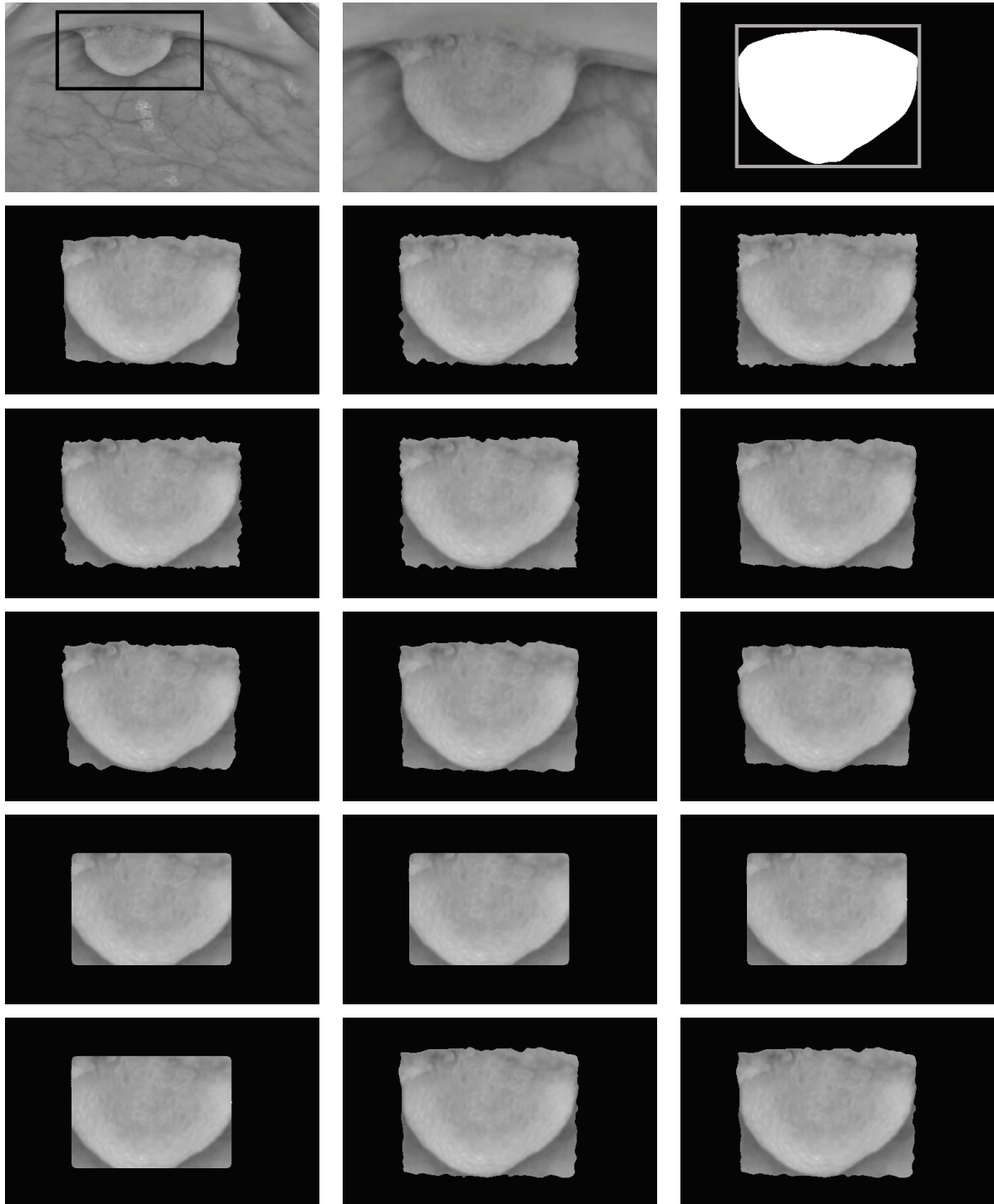


Fig. 3. The masks resulting from the geodesic method for one input image with different prefiltering methods. The original input image is the background subtracted image (65) in ETIS-Larib Polyp DB database (Juan et al., 2014); it appears in the top left, in position 1), next, in position 2) is the zoomed version of the original, unfiltered image for better visualization (indicated in image 1) by a black rectangle), and 3) the ground truth mask belonging to the zoomed partion; the gray rectangle denotes the initial mask boundaries we used in the calculation.

The order of appearance for the geodesic masks: 4) original, unfiltered image, 5-8) Gradient filtered images (magnitude, direction,  $x$  and  $y$  component), 9) mean filtered image, 10) standard deviation filtered image, 11) median filtered image, 12) difference of mean and median filtered image, 13)  $S_1$ , 14)  $S_2$ , 15)  $S_{sr}$ , 16)  $\ln q$  filtered images, 17) Gaussian filtered image, and 18) Wiener filtered image.

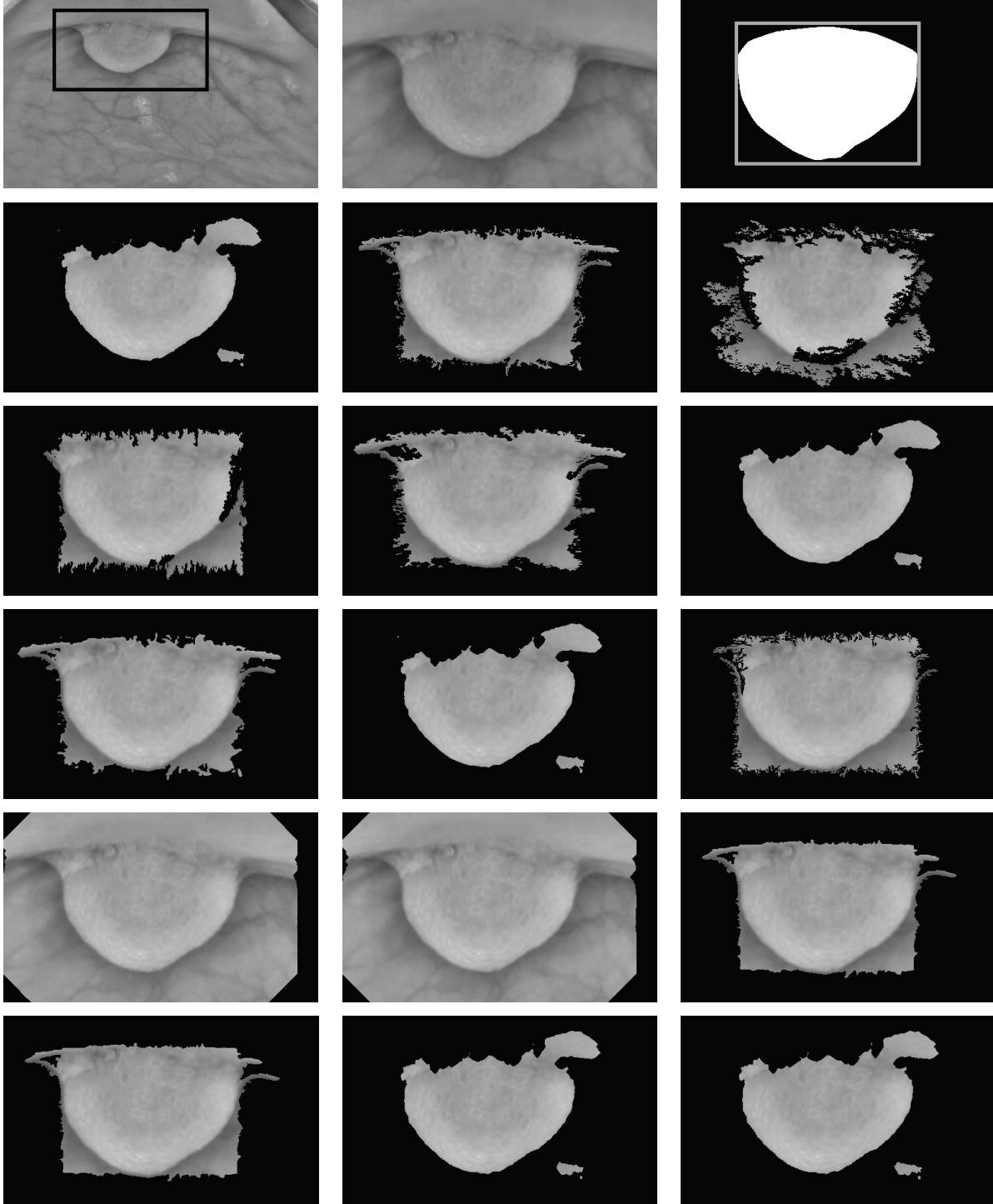


Fig. 4. The masks resulting from the Chan–Vese method for one input image with different prefiltering methods. The original input image is the background subtracted image (65) in ETIS-Larib Polyp DB database (Juan et al., 2014); it appears in the top left, in position 1), next, in position 2) is the zoomed version of the original, unfiltered image for better visualization (indicated in image 1) by a black rectangle), and 3) the ground truth mask belonging to the zoomed partion; the gray rectangle denotes the initial mask boundaries we used in the calculation.

The order of appearance for the Chan–Vese masks: 4) original, unfiltered image, 5-8) Gradient filtered images (magnitude, direction, x and y component), 9) mean filtered image, 10) standard deviation filtered image, 11) median filtered image, 12) difference of mean and median filtered image, 13)  $S_1$ , 14)  $S_2$ , 15)  $S_{str}$ , 16)  $\ln q$  filtered images, 17) Gaussian filtered image, and 18) Wiener filtered image.

## CIRCULAR ACTIVE CONTOUR INITIAL MASK CASE

In order to investigate whether a different shape of the initial mask will influence the performance of geodesic and Chan–Vese methods, we suggested using a circular initial mask instead of the first rectangular one, because in some cases the rough polyp finding algorithms (like the Hough transform based ones) provide a circle as an output.

For this purpose, we evaluated three circular initial masks with the same center which is the center of the rectangular mask previously used, and different diameters. The width, length, and diameter of the rectangular mask have been tested as three proposed diameters for the circular initial mask. The most reasonable results were achieved using a circular mask with a diameter equals to the length of the first rectangular mask, so we will present and discuss only its results in this paper.

We compared Sørensen–Dice similarity coefficient values for each method using both rectangular and circular initial masks and default parameters for the five

selected input images. The comparison results are numerically listed in the three tables of the appendix and illustrated as charts in Fig. 5.

The geodesic comparison results showed that about (91.67%) of the total similarity coefficients was higher in the case of using the rectangular initial mask. Whereas the circular initial mask worked better only with (8.33%) of the coefficients. Furthermore, the Chan–Vese results indicated that the use of the rectangular initial mask was approximately better with (50%) of the total similarity coefficients and the circular initial mask was more fit for the remaining (50%) of the coefficients. Based on previously clarified results, the Chan–Vese method demonstrated adaptability to the shape of the initial mask more than the geodesic method.

## MODIFIED RECTANGULAR INITIAL MASK AND TUNED PARAMETERS CASE

The effect of the rectangular initial mask size with the tuned parameters was verified in this case. We proposed initializing the geodesic and Chan–Vese with two different masks and different parameters. The geodesic method was initialized using the same rectangular mask

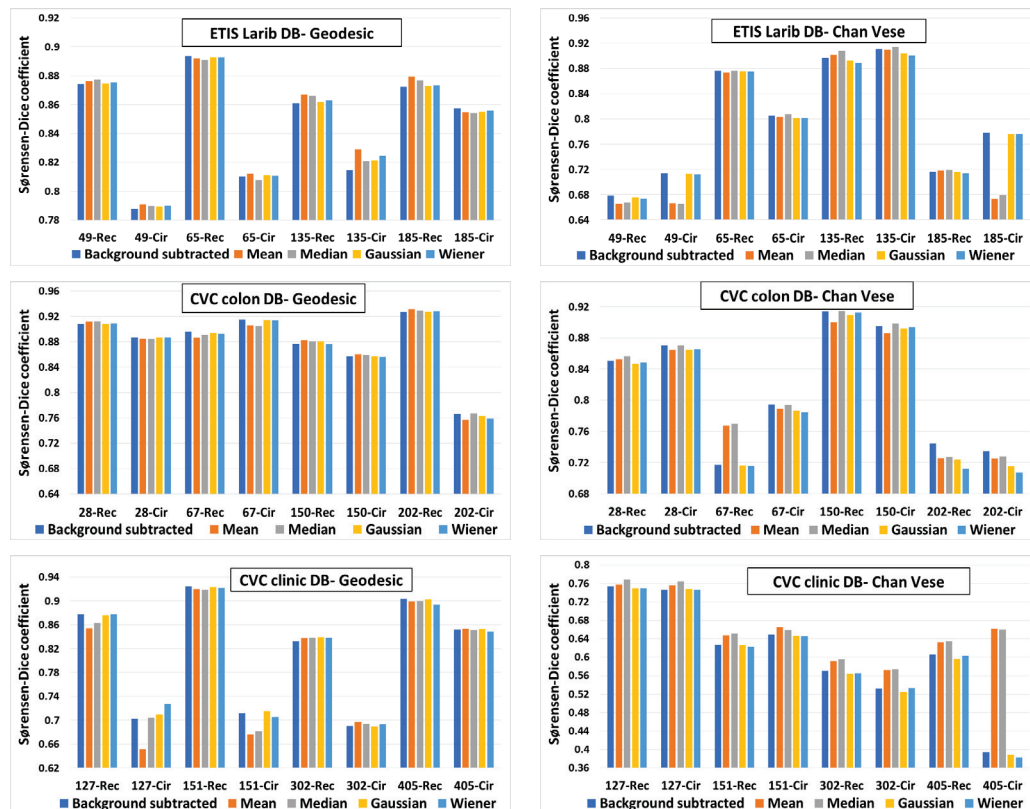


Fig. 5. Sørensen–Dice similarity coefficient comparison results for geodesic and Chan–Vese methods using both rectangular and circular initial masks for the image samples of the three studied databases (Juan et al., 2014; Bernal et al., 2012; 2015). The rectangular and circular masks are indicated by (Rec) and (Cir) respectively. The order of the columns' colours is in the same order as in the bottom of the figures: background subtracted, mean, median, Gaussian and Wiener filtered images.

which encompasses the polyp area, whereas the Chan–Vese method was initialized using a decreased size rectangular mask located within the polyp area.

Since the smoothness factor parameter modifies the contour length penalty, which makes a trade-off between fitting the fine details of the input image more precisely with a smaller smoothness value vs. giving a smoother segmented contour with a larger value. Whereas the contraction bias parameter defines the penalty (if it has a positive value) or reward (if it has a negative value) for

the area inside the initial contour. We empirically selected the previously discussed parameters. The geodesic method continued to work well with the same default parameters, i.e., the smoothness factor is 1 and the contraction bias is 0.3. While the Chan–Vese method worked better with a smoothness factor equals to 1, and contraction bias equals  $-0.5$ . We evaluated the performance of both methods using the different initial masks and different parameters for 100, 200, and 300 iterations. Figures 6, 7 and 8 illustrate the overall results of this case. Table 2 gives one numerical sample from the results.

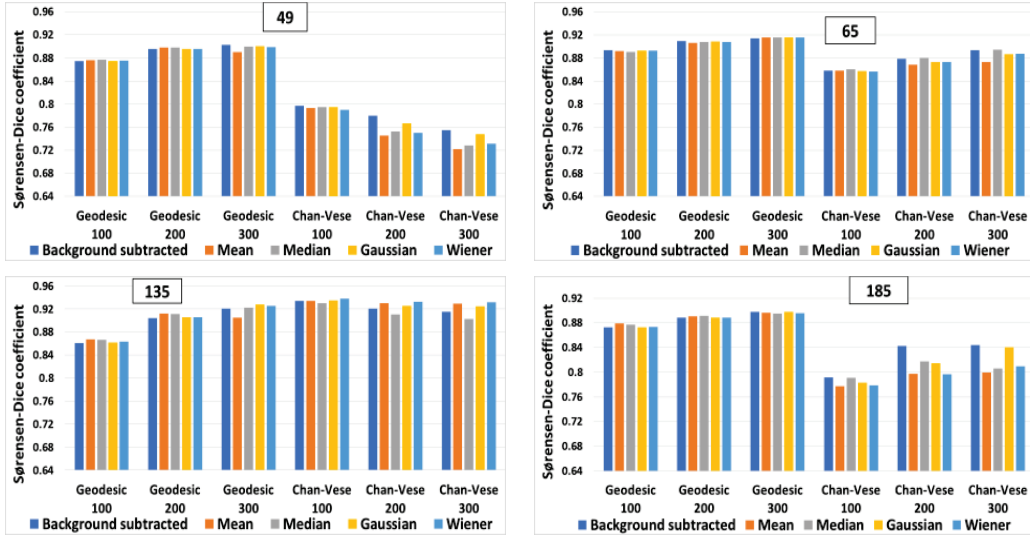


Fig. 6. *Sørensen–Dice Coefficient of the modified rectangular initial mask and tuned parameters case for the image samples in ETIS-Larib Polyp DB database (Juan et al., 2014), with 100, 200, and 300 iterations. The order of the columns’ colours is in the same order as in the bottom of the figures: background subtracted, mean, median, Gaussian and Wiener filtered images.*

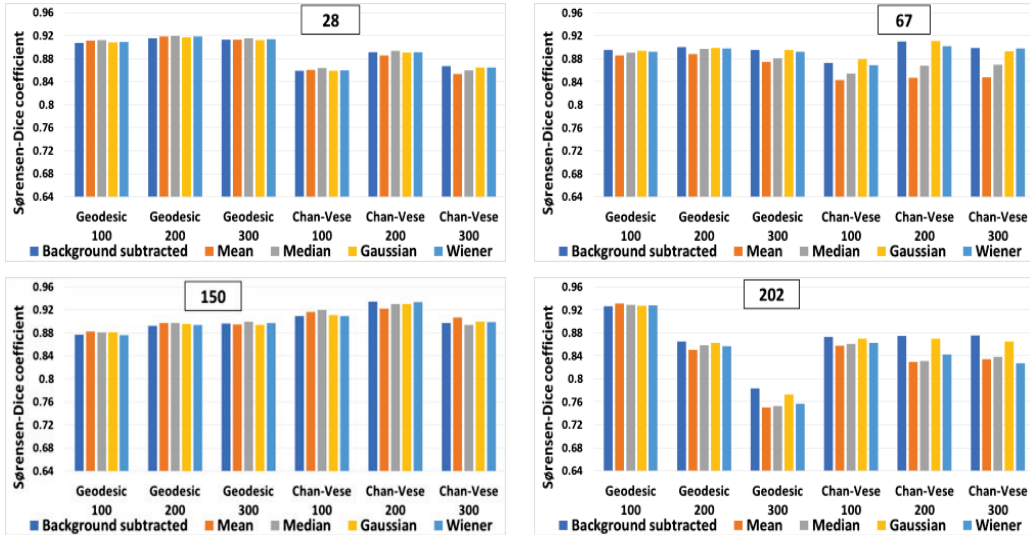


Fig. 7. *Sørensen–Dice Coefficient of the modified rectangular initial mask and tuned parameters case for the image samples in CVC-ColonDB database (Bernal et al., 2012), with 100, 200, and 300 iterations. The order of the columns’ colours is in the same order as in the bottom of the figures: background subtracted, mean, median, Gaussian and Wiener filtered images.*

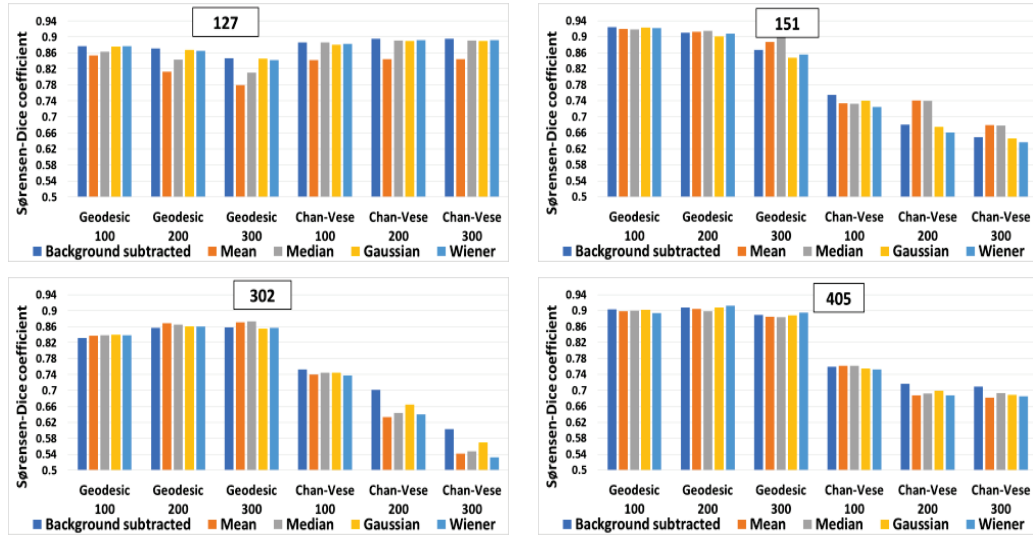


Fig. 8. Sørensen–Dice Coefficient of the modified rectangular initial mask and tuned parameters case for the image samples in CVC-ClinicDB database (Bernal *et al.*, 2015), with 100, 200, and 300 iterations. The order of the columns' colours is in the same order as in the bottom of the figures: background subtracted, mean, median, Gaussian and Wiener filtered images.

Table 2. Numerical values for Sørensen–Dice Coefficient of the modified rectangular initial mask and tuned parameters case for the image sample (151) in CVC-ClinicDB database (Bernal *et al.*, 2015), with 100, 200, and 300 iterations. The highlighted values refer to the Chan–Vese improved values compared with the post pre-processing results given in the appendix Table A3.

Image Number	Active Contour Input Image	Geodesic 100	Geodesic 200	Geodesic 300	Chan–Vese 100	Chan–Vese 200	Chan–Vese 300
151	Background subtracted	0.9246	0.9100	0.8674	0.7552	0.6810	0.6496
	Mean	0.9198	0.9127	0.8867	0.7338	0.7412	0.6792
	Median	0.9185	0.9154	0.8994	0.7332	0.7400	0.6778
	Gaussian	0.9234	0.9007	0.8473	0.7403	0.6753	0.6454
	Wiener	0.9217	0.9083	0.8554	0.7249	0.6607	0.6370

In the case of 100 iterations and in comparison with the post pre-processing case with rectangular initial mask results, the geodesic method results remained the same in this sub-case because we used the same mask and parameters. Regarding the Chan–Vese method, about (88.34%) of the total similarity coefficients improved with the modified rectangular initial mask and tuned parameters case. As an example to show the evolution of the results, Fig. 9 compares the Chan–Vese segmentation results of the image (135) in ETIS-Larib Polyp DB database (Juan *et al.*, 2014), in both the post-pre-processing with rectangular initial mask and the modified rectangular initial mask and tuned parameters cases with 100 iterations.

From the results previously discussed and for the majority of the image samples, the geodesic approach

achieved the best performance using the initial mask which surrounds the boundaries of the polyp to be segmented with a contraction bias value which makes the contour shrink towards the polyp area. While the Chan–Vese approach accomplished the best results using the initial mask located inside the polyp area with a contraction bias value which makes the contour expand towards the polyp.

The results of the segmentation methods with higher number of iterations (200 and 300) varied according to the used pictures and to the different not uniform characteristics of the databases. The difference in the studied image size in the different databases and the variation of the polyp size compared to its image size is one of the most important reasons for the results' inconsistent tendency. The polyp shape (elliptical, circular, irregular...),

the polyp viewpoint (top view, lateral, semi lateral), and the strength of the polyp's edges are additional factors that can together lead to this irregular performance. Another important note is that the masks given by the databases were drawn manually and some of them did not match the borderline of the polyps perfectly, thus if our method went closer to the ideal contour than the manually drawn mask, then the Sørensen–Dice metric showed a worse result than expected.

For the ETIS-Larib Polyp DB database (Juan *et al.*, 2014) images which have the largest size, the improvement in the performance of the geodesic method with increasing the iterations number was evident in (38 out of 40) values of the total similarity coefficients in the case of 200 and 300 iterations. The Chan–Vese method improved just for (19) values of the total coefficients. However, as the decrease in the performance of the Chan–Vese method in the case of image 49 was due to a reflection at the borderline of the polyp, a general conclusion can be drawn; the higher number of iterations is optimal for this database.

For CVC-ColonDB database (Bernal *et al.*, 2012) images which have a medium size, most of the similarity coefficients values increased in the case of 200 iterations, (15 out of 20) and (17 out of 20) for the geodesic and Chan–Vese methods respectively. Then a decrease followed in the case of 300 iterations: (17 out of 20) and (15 out of 20) of the total similarity coefficients values decreased using the geodesic and Chan–Vese methods respectively. In this case, the 200 iterations seem to be an optimum. The exception for this tendency is image 202, where the edges were not strong, and the image is blurry, thus the geodesic method cannot really find optimum.

For CVC-ClinicDB database (Bernal *et al.*, 2015) images which have the smallest size, (70%) and (75%) of the total similarity coefficients became lower in the case of applying 200 and 300 iterations compared to the case of 100 iterations with the geodesic and Chan–Vese methods respectively. Here, less clearly than in the previous case, the 100 iterations seem to be the optimal choice.

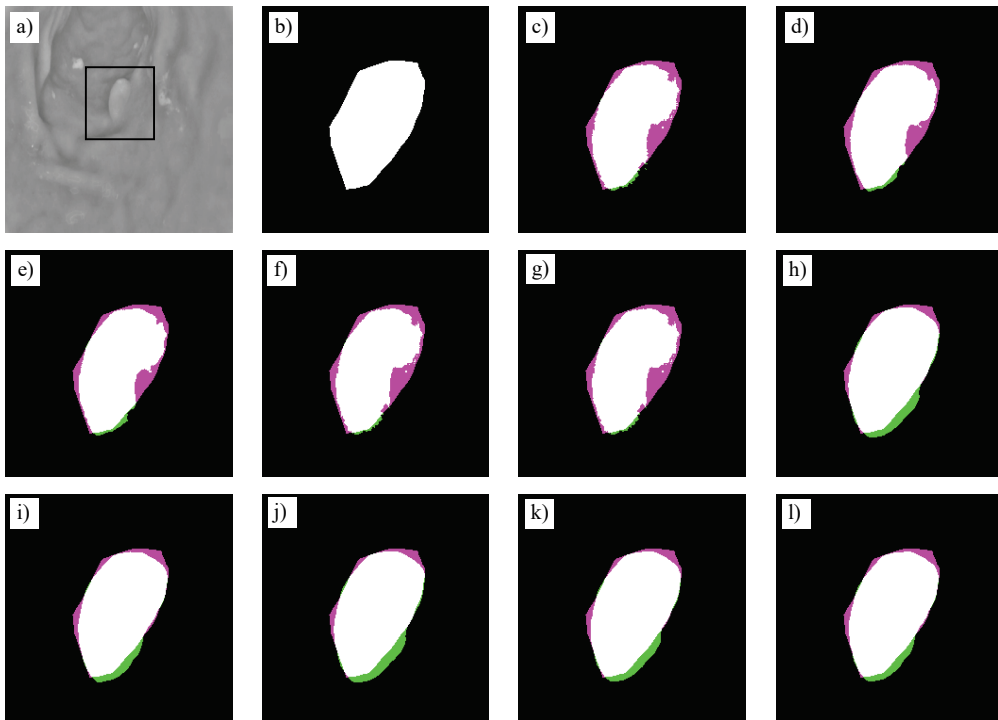


Fig. 9. The Chan–Vese comparison segmentation results of the image (135) in ETIS-Larib Polyp DB database (Juan *et al.*, 2014). (a) The original background subtracted image, with the zoomed part indicated by a black square around the polyp. (b) The given database mask. (c, e, g, i, k) The original (unfiltered image), mean, median, Gaussian, and Wiener filtered images results in the post pre-processing with rectangular initial mask case. (d, f, h, j, l) The original (unfiltered image), mean, median, Gaussian, and Wiener filtered images results in the modified rectangular initial mask and tuned parameters case with 100 iterations. The colours connotations: white is the matching area between the given database mask and the resulted segmented area, pink is the remaining area of the given mask that was not covered by the segmented area, and green is an additional area of the segmented area.

## SPECIAL CASES

We studied some special cases, as an extension of our experiments.

Firstly, we studied what happens if the masks are not located around the polyps. Using the same previous studied image samples, the performance of three alternative initial mask locations was tested.

In the first case, the starting mask was initialized around some fairly smooth region far away from the polyp area to be segmented. This case produced undesired segmentation results, the geodesic method could not find any contour to shrink on, so it remained more or less the same as the initial mask. In the case of the Chan–Vese method, the resulting masks were mostly covering one or multiple regions between visible veins or folds, and the method failed both to find the polyp, and to indicate that the mask is located in a wrong area.

In the second case, when the initial and ground-truth masks only partially overlapped, the Chan–Vese method expanded toward the polyp area. However, if one or more, fairly homogeneous area was included into the initial mask, it kept evolving towards these areas, too, and they remained as separate parts of the result. The geodesic method, similarly to the first case (without overlap), did not change much compared to the initial mask, only on the side of the polyp, if the borderlines were strong enough.

If multiple polyps were present in the image, and the initial mask was one joint mask instead of two separate ones, the methods also failed to find the polyps. In the case of multiple polyps, at least one of the polyps had only partially visible borderlines, and very similar colour to the background. As more prominent edges and colour regions were due to the folding of the bowel than due to the polyps themselves, these methods were not suitable to separate them, even if theoretically they can distinguish multiple objects.

These studies showed the sensitivity of the methods to the initial contour location.

As a next step, the colour sensitivity was studied. In the case of an advanced stage polyp, the polyp colour is different from the colour of the background, whereas in early stages, the polyp and the background usually have the same colour. For darker coloured polyps, even the background subtraction is not necessary, the methods find the polyps rather well for both the original, and the background subtracted images. As an example of an advanced stage colorectal polyp, the results for image sample 516 with dark polyp from the CVC-ClinicDB database (Bernal *et al.*, 2015) are shown in Figure 10. The

other examples in the articles were all on images with polyps having the same colour as the bowel around them.

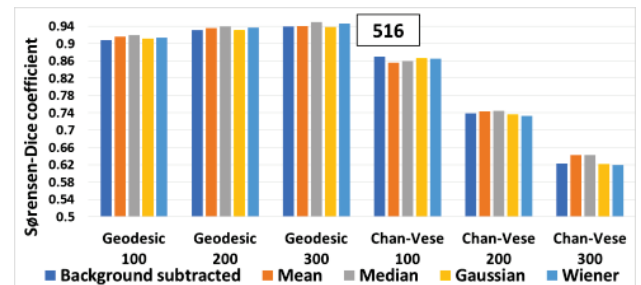


Fig. 10. *Darker polyp example: image sample 516 in CVC-ClinicDB database (Bernal et al., 2015). Sørensen–Dice Coefficient of the modified rectangular initial mask and tuned parameters case with 100, 200, and 300 iterations. Separate initial masks were used for the Chan–Vese and for the geodesic method. The order of the columns’ colours is in the same order as in the bottom of the figures: background subtracted, mean, median, Gaussian and Wiener filtered images.*

## DISCUSSION

In this paper, the geodesic and Chan–Vese active contours were explored as two methods to segment the polyps in 16 image samples of the ETIS-Larib Polyp DB, CVC-ColonDB, CVC-ClinicDB colonoscopy databases.

For implementation, pre-processing steps were applied to eliminate the undesirable reflections and obtain a background-subtracted version of the studied images. Pre-processing steps were followed by testing the outputs of 14 different pre-filtering methods as potential inputs for the active contour methods. Mean, median, Gaussian, and Wiener filtered images were selected for further study, due to their good segmentation results with both geodesic and Chan–Vese methods.

Circular and rectangular initial masks were used to investigate the effect of the initial mask shape on the segmentation results. The Chan–Vese method showed more flexibility with respect to the difference of the initial mask shape compared to the geodesic method.

Finally, modified rectangular initial mask and tuned parameters cases were studied to verify the effect of the initial mask size and parameter selection on the results. The best performance for the geodesic method was achieved using an initial mask encompassed the polyp area, whereas an initial mask located within the polyp region proved to be the most appropriate choice for the Chan–Vese method. The necessary number of iterations depended a lot on various factors, on the size of the image and the polyp, the edge intensity and the view point

compared to the polyps, the visibility of the veins around the polyp, the compensated reflections and their location, but no clear correlation to any of these factors could be found.

In most of the cases, the Chan–Vese method performed better than the geodesic method in matching the contour of the actual polyps, but it depended more on the effectiveness of the pre-processing procedure.

## REFERENCES

- Adams R, Bischof L (1994). Seeded region growing. *IEEE TRANS PATTERN ANAL MACH INTELL* 16 (6):641–7.
- Bernal J, Sanchez F J, Vilarino F (2012). Towards Automatic Polyp Detection with a Polyp Appearance Model. *PATTERN RECOGNIT* 45:3166–82.
- Bernal J, Sánchez FJ, Fernández-Esparrach G, Gil D, Rodríguez C, Vilarino F (2015). WM-DOVA maps for accurate polyp highlighting in colonoscopy: Validation vs. saliency maps from physicians. *COMPUT MED IMAGING GRAPH* 43:99–111.
- Bernal J, *et al.* (2017). Comparative Validation of Polyp Detection Methods in Video Colonoscopy: Results from the MICCAI 2015 Endoscopic Vision Challenge. *IEEE TRANS MED IMAGING*, 36:1231–49.
- Bhat S H, Kumar P (2019). Segmentation of Optic Disc by Localized Active Contour Model in Retinal Fundus Image. In M. C. Trivedi, *et al.* (Eds.), *Smart Innovations in Communication and Computational Sciences*; Springer Verlag 851:35–44.
- Brice Claude R, Fennema Claude L (1970). Scene Analysis Using Regions. Technical Note 17. AI Center, SRI International, 333 Ravenswood Ave, Menlo Park, CA 94025, April.
- Canny J (1986). A Computational Approach to Edge Detection. *IEEE TRANS PATTERN ANAL MACH INTELL* 8(6):679–98.
- Carass A, Roy S, Gherman A. *et al* (2020). Evaluating White Matter Lesion Segmentations with Refined Sørensen-Dice Analysis. *SCI REP* 10:8242.
- Caselles V, Kimmel R, Sapiro G (1997). Geodesic Active Contours. *INT J COMPUT VIS* 22:61–79.
- Chan T, Vese L (2000). Image segmentation using level sets and the piecewise-constant Mumford-Shah model. Tech. Rep. 0014, Computational Applied Math Group.
- Chan T, Vese L (2001). Active contours without edges. *IEEE TRANS IMAGE PROCESS* 10:266–277.
- Dervieux A, Thomasset F (1979). A finite element method for the simulation of Rayleigh–Taylor instability. Rautman, R. (ed.) *Approximation Methods for Navier–Stokes Problems*. Lecture Notes in Mathematics Berlin; Springer, 771:145–158.
- Dutta S, Sasmal P, Bhuyan M K, Iwahori Y (2018). Automatic Segmentation of Polyps in Endoscopic Image Using Level-Set Formulation. 2018 International Conference on Wireless Communications, Signal Processing and Networking (WiSPNET), Chennai; 1–5.
- Fang L, Pan X, Yao Y. *et al* (2020). A hybrid active contour model for ultrasound image segmentation. *SOFT COMPUT* 24:18611–25.
- Georgieva V, Petrov P (2017). An Approach for Colorectal Polyp Segmentation. Conference on Communication, Electromagnetics and Medical Application (CEMA'2017), Sofia, Bulgaria, October.
- Georgieva V, Petrov P, Nagy S, Sziová, B (2018). Detecting contours of pathological forms in colonoscopy images using a hybrid method. Proceedings of 13th International Conference on Communication, Electromagnetics and Medical Application (CEMA'2018) October 2018, Sofia, Bulgaria.
- Ismail R, Nagy S (2021). On Metrics Used in Colonoscopy Image Processing for Detection of Colorectal Polyps. In: *New Approaches for Multidimensional Signal Processing, Smart Innovation, Systems and Technologies*; Springer Singapore, Chapter 10, 216:137–51.
- Juan S S, Aymeric H, Olivier R, Xavier D, Bertrand G (2014). Towards Embedded Detection of Polyps in WCE Images for Early Diagnosis of Colorectal Cancer. *INT J COMPUT ASSIST RADIOLOG SURG* 9(2): 283–93.
- Kass M, Witkin A, Terzopoulos D (1988). Snakes: Active contour models. *INT J COMPUT VISION* 1, 321–31.
- Kichenassamy S, Kumar A, Olver P, Tannenbaum A, Yezzi A (1995). Gradient flows and geometric active contour models. Anon (Ed.), *IEEE International Conference on Computer Vision*; 810–15.
- Mumford D, Shah J (1989). Optimal approximations by piecewise smooth functions and associated variational problems. *COMMUN PURE APPL MATH* 42(5): 577–685.
- Nagy S, Sziová B, Solecki L (2020). The effect of background and outlier subtraction on the structural entropy of two-dimensional measured data. *INT J REASON-BASED INTELL SYST* 12 (3): 200–9.
- Nagy Sz, Lilik F, Kóczy L T (2017). Entropy based fuzzy classification and detection aid for colorectal polyps. *IEEE Africon 2017*, Cape Town, South Africa, September.
- Nguyen N, Vo D M, Lee S (2020). Contour-Aware Polyp Segmentation in Colonoscopy Images Using Detailed Upsampling Encoder-Decoder Networks. *IEEE ACCESS* 8: 99495–508.
- Osher S, Sethian J A (1988). Fronts Propagation with Curvature Dependent Speed: Algorithms Based on Hamilton Jacobi Formulations. *J COMPUT PHYS* 79(1): 12–49.

- Pipek J, Varga I (1992). Universal classification scheme for the spatial-localization properties of one-particle states infinite, d-dimensional systems. *PHYS REV A*, 46: 3148–63.
- Rényi A (1960). On measures of information and entropy. Proceedings of the fourth Berkeley Symposium on Mathematics, Statistics and Probability, Berkeley, CA, USA, 20 June–30 July 547–61.
- Sasmal P, Iwahori Y, Bhuyan M K, Kasugai K (2018). Active contour segmentation of polyps in capsule endoscopic images. 2018 International Conference on Signals and Systems (ICSigSys) Bali 2018 201–4.
- Shannon C E (1948). A mathematic theory of communication. *BELL SYSTE TECH J* 27: 379–423.
- Taha A A, Hanbury A (2015). Metrics for evaluating 3D medical image segmentation: analysis, selection, and tool. *BMC MED IMAGING* 15:29.
- Yang X, Jiang X (2020). A Hybrid Active Contour Model based on New Edge-Stop Functions for Image Segmentation. *INT J AMBIENT COMPUT INTELL* 11: 87–98.
- Yuji I, Akira H, Yoshinori A, Bhuyan M, Robert J, Kunio K (2015). Automatic Detection of Polyp Using Hessian Filter and HOG Features. 19th International Conference in Knowledge Based and Intelligent Information and Engineering Systems - KES2015, *PROCEEDIA COMPUT SCI* 60: 730–9.

## APPENDIX

Sørensen–Dice Coefficient of the post pre-processing case for the image samples in the three studied databases, with both rectangular and circular initial

masks. The highlighted value indicates the value that improved after the pre-processing steps.

Table A1. *Sørensen–Dice Coefficient of the post pre-processing case for the image samples in ETIS-Larib Polyp DB database (Juan et al., 2014)*

Image Number	Active Contour Input Image	Geodesic Rectangular	Geodesic Circular	Chan–Vese Rectangular	Chan–Vese Circular
49	Background subtracted	0.8743	0.7879	0.6787	0.7137
	Mean	0.8763	0.7910	0.6661	0.6662
	Median	0.8773	0.7897	0.6678	0.6655
	Gaussian	0.8745	0.7892	0.6761	0.7129
	Wiener	0.8755	0.7902	0.6737	0.7122
65	Background subtracted	0.8937	0.8102	0.8763	0.8047
	Mean	0.8921	0.8121	0.8736	0.8028
	Median	0.8908	0.8079	0.8760	0.8074
	Gaussian	0.8929	0.8111	0.8755	0.8017
	Wiener	0.8927	0.8107	0.8747	0.8020
135	Background subtracted	0.8610	0.8148	0.8969	0.9111
	Mean	0.8669	0.8290	0.9016	0.9098
	Median	0.8660	0.8208	0.9080	0.9140
	Gaussian	0.8618	0.8212	0.8923	0.9044
	Wiener	0.8630	0.8247	0.8890	0.9001
185	Background subtracted	0.8724	0.8574	0.7167	0.7786
	Mean	0.8793	0.8547	0.7184	0.6730
	Median	0.8768	0.8542	0.7190	0.6791
	Gaussian	0.8730	0.8551	0.7155	0.7763
	Wiener	0.8735	0.8559	0.7137	0.7763

Table A2. *Sørensen–Dice Coefficient of the post pre-processing case for the image samples in CVC-ColonDB database (Bernal et al., 2012)*

Image Number	Active Contour Input Image	Geodesic Rectangular	Geodesic Circular	Chan–Vese Rectangular	Chan–Vese Circular
28	Background subtracted	0.9080	0.8867	0.8503	0.8702
	Mean	0.9117	0.8848	0.8527	0.8644
	Median	0.9122	0.8845	0.8562	0.8702
	Gaussian	0.9084	0.8867	0.8470	0.8641
	Wiener	0.9090	0.8870	0.8482	0.8651
67	Background subtracted	0.8960	0.9149	0.7172	0.7943
	Mean	0.8863	0.9053	0.7674	0.7893
	Median	0.8907	0.9049	0.7694	0.7938
	Gaussian	0.8941	0.9144	0.7162	0.7867
	Wiener	0.8925	0.9133	0.7157	0.7845
150	Background subtracted	0.8772	0.8572	0.9140	0.8948
	Mean	0.8823	0.8605	0.8998	0.8861
	Median	0.8808	0.8589	0.9146	0.8981
	Gaussian	0.8808	0.8572	0.9091	0.8916
	Wiener	0.8764	0.8565	0.9122	0.8940
202	Background subtracted	0.9266	0.7665	0.7447	0.7345
	Mean	0.9314	0.7567	0.7257	0.7252
	Median	0.9287	0.7666	0.7272	0.7279
	Gaussian	0.9274	0.7632	0.7242	0.7150
	Wiener	0.9283	0.7590	0.7118	0.7072

Table A3. *Sørensen–Dice Coefficient of the post pre-processing case for the image samples in CVC-ClinicDB database (Bernal et al., 2015).*

<b>Image Number</b>	<b>Active Contour Input Image</b>	<b>Geodesic Rectangular</b>	<b>Geodesic Circular</b>	<b>Chan–Vese Rectangular</b>	<b>Chan–Vese Circular</b>
<b>127</b>	<b>Background subtracted</b>	0.8769	0.7024	0.7541	0.7461
	<b>Mean</b>	0.8537	0.6510	0.7576	0.7558
	<b>Median</b>	0.8626	0.7039	0.7684	0.7646
	<b>Gaussian</b>	0.8757	0.7094	0.7493	0.7476
	<b>Wiener</b>	0.8770	0.7275	0.7492	0.7464
<b>151</b>	<b>Background subtracted</b>	0.9246	0.7117	0.6275	0.6496
	<b>Mean</b>	0.9198	0.6762	0.6473	0.6658
	<b>Median</b>	0.9185	0.6814	0.6514	0.6589
	<b>Gaussian</b>	0.9234	0.7152	0.6262	0.6465
	<b>Wiener</b>	0.9217	0.7055	0.6225	0.6455
<b>302</b>	<b>Background subtracted</b>	0.8317	0.6906	0.5705	0.5327
	<b>Mean</b>	0.8375	0.6970	0.5921	0.5723
	<b>Median</b>	0.8383	0.6939	0.5953	0.5739
	<b>Gaussian</b>	0.8391	0.6899	0.5641	0.5247
	<b>Wiener</b>	0.8383	0.6931	0.5654	0.5335
<b>405</b>	<b>Background subtracted</b>	0.9032	0.8522	0.6065	0.3941
	<b>Mean</b>	0.8990	0.8531	0.6330	0.6621
	<b>Median</b>	0.8998	0.8514	0.6342	0.6603
	<b>Gaussian</b>	0.9026	0.8526	0.5964	0.3891
	<b>Wiener</b>	0.8937	0.8482	0.6036	0.3832